Catalysis Today xxx (xxxx) xxx–xxx

Contents lists available at ScienceDirect

Catalysis Today

journal homepage: www.elsevier.com/locate/cattod

Bio-hydrogen production by APR of C_2-C_6 polyols on Pt/Al_2O_3: Dependence of H_2 productivity on metal content

H.A. Duarte, M.E. Sad, C.R. Apesteguía*

Catalysis Science and Engineering Research Group (GICIC), INCAPE, UNL-CONICET, Predio CCT Conicet, Paraje El Pozo, Santa Fe, 3000, Argentina

ARTICLE INFO

Keywords:
Bio-hydrogen
Aqueous-phase reforming
Polyol APR
Pt/Al_2O_3 catalysts
H_2 production

ABSTRACT

The effect of the platinum loading on the production of hydrogen by aqueous-phase reforming of ethylene glycol, glycerol, xylitol and sorbitol was studied on Pt/Al_2O_3 catalysts containing 0.30, 0.57, 1.50 and 2.77 Pt%. Catalytic runs were performed at a space velocity of 1.2 h^{-1}, 498 K, 29.3 bar and using a polyol(1.0%)/water feed. The total polyol conversion and the polyol conversion to gaseous products increased with surface Pt concentration (Pt_s, μmol Pt/g_{cat}). Similarly, the yield and the productivity to hydrogen (*Pr*, mol H_2/g h) increased continuously with Pt_s in all the cases, but the *Pr* values diminished with the polyol chain length. Coke formation depended on Pt_s and the polyol size; the amount of carbon formed on the catalyst increased indeed with Pt_s and diminished with the polyol chain length. The metal fraction was severely sintered during the APR reaction, irrespective of the reactant size. Nevertheless, the magnitude of the Pt dispersion drop was not dependent on the amount of platinum on Pt/Al_2O_3 catalysts.

1. Introduction

Reforming of biomass-derived compounds in aqueous phase (APR) is a promising technology to produce bio-hydrogen, a renewable energetic carrier that is also used for producing valuable chemicals [1,2]. The APR process was introduced by Dumesic's group in 2002 aiming the production of hydrogen from polyols, sugars and sugar alcohols obtained from lignocellulosic biomass [3]. The process generates hydrogen with low amounts of CO in a single reactor at low temperatures (423 K–543 K) and moderate pressures (15–40 bar), which avoids the costs of water vaporization and favors the purification of the hydrogen effluent stream [4,5]. The production of bio-hydrogen was initially investigated for APR of polyols with shorter carbon chains such as ethylene glycol and glycerol [6–9]. Then, the APR of larger sugar alcohols (sorbitol, xylitol) and sugars (glucose) were also studied [10–14]. The conversion of biomass-derived oxygenated hydrocarbons to hydrogen is characterized by a complex chemistry, especially as the size of the substrate increases.

The direct reaction pathway to produce H_2 via APR of polyols involves the C—C as well as C—H and O—H bond scissions on the catalyst surface to form adsorbed CO that consecutively yields CO_2 and H_2 via the water-gas shift (WGS) reaction. As an example, Fig. 1 shows a simplified scheme accounting for the production of hydrogen via the APR of glycerol. For a polyol containing *n* carbon atoms (polyol P_n) the APR reaction pathway involves the initial reactant decarbonylation (reaction 1) followed by the WGS reaction (reaction 2). The formation stoichiometry of H_2 and CO_2 from polyol P_n is represented by reaction 3:

$$C_nO_nH_{2n+2} \rightarrow n\ CO + (n+1)\ H_2 \quad (1)$$

$$n\ CO + n\ H_2O \rightarrow n\ CO_2 + n\ H_2 \quad (2)$$

$$C_nO_nH_{2n+2} + n\ H_2O \rightarrow n\ CO_2 + (2n+1)\ H_2 \quad (3)$$

Significant formation of byproducts may occur in the APR of polyols, in particular via parallel reactions involving cleavage of C—O bonds that leads to formation of side products such as alkanes and alcohols [11,15]. In the gas phase, formation of methane by hydrogenation of CO and CO_2 is also an undesired side reaction. Development of catalysts that selectively promote the C—C bond cleavage and water-gas shift reaction is therefore a requisite for efficiently generating H_2 from APR of polyols. Platinum supported on alumina or carbon has been widely employed for the APR reaction [3,9,10,13,16]. In this regard, previous studies have shown that Pt is more selective than other metals [17] and that the moderate acidity of alumina or carbon does not favor the undesired acid catalyzed dehydration of the substrate to liquid products [18]. Platinum is a high-priced metal of limited availability and is therefore important to determine the optimal Pt content required to achieve the highest H_2 productivity. However, very few studies addressing the relationship between the Pt loading and the

* Corresponding author at: INCAPE, Predio CCT Conicet, Paraje El Pozo, Santa Fe, 3000, Argentina.
E-mail addresses: capesteg@gmail.com, capesteg@fiq.unl.edu.ar (C.R. Apesteguía).

http://dx.doi.org/10.1016/j.cattod.2017.04.067
Received 6 February 2017; Received in revised form 20 March 2017; Accepted 30 April 2017

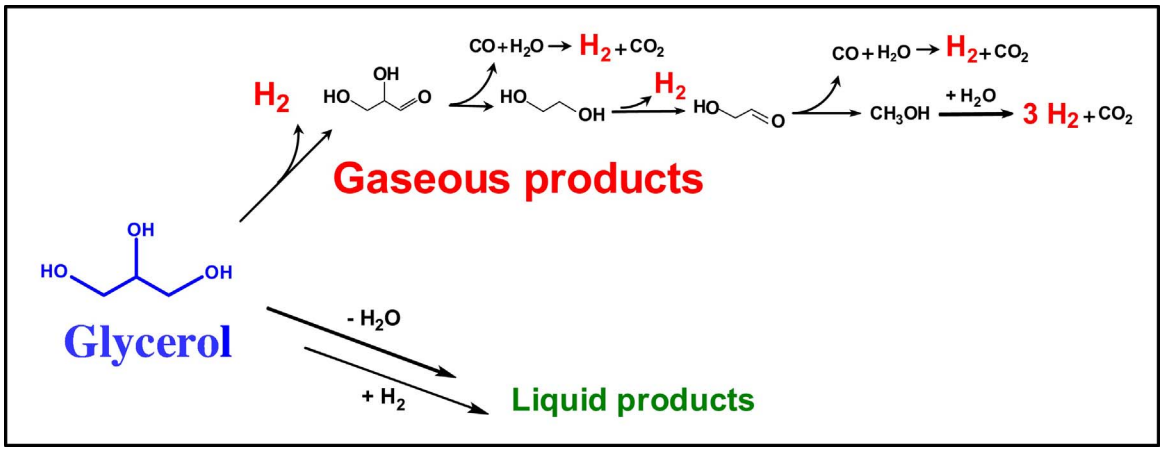

Fig. 1. Simplified scheme of H_2 production via APR of glycerol.

H_2 productivity for APR of polyols on Pt-supported catalysts have been reported. In particular, no reports were published so far on the effect of Pt content on the formation of coke and catalyst deactivation in aqueous phase reforming of polyols. The structure sensitivity of the APR of glycerol and ethylene glycol was investigated by varying the Pt particle size on platinum supported on alumina or carbon [8,19,20]. Recently, we used Pt/Al_2O_3 catalysts containing different %Pt to investigate the effect of the Pt content on the production of H_2 for the APR of sorbitol [21]. Here, we have extended these studies on Pt/Al_2O_3 catalysts to stablish and compare the effect of Pt surface concentration on the catalyst activity, selectivity and stability for the APR of ethylene glycol (EG), glycerol (Gly), xylitol (Xyl) and sorbitol (Sorb). Results show that at a given space velocity, the H_2 yield and productivity as well as the amount of coke formed on the catalyst depend essentially on the Pt surface concentration and the polyol size.

2. Experimental

2.1. Catalyst preparation and characterization

Four Pt/Al_2O_3 catalysts containing different Pt contents were prepared and are identified here as catalysts I (0.30 Pt%), II (0.57 Pt %), III (1.50 Pt%) and IV (2.77 Pt%). All the catalysts were prepared by incipient-wetness impregnation at 303 K of a high-purity γ-Al_2O_3 powder (Cyanamid Ketjen CK300) with an aqueous solution of tetra-amine platinum nitrate, $Pt(NH_3)_4(NO_3)_2$ (Aldrich, 99.99%). The CK300 alumina had BET surface area of 220 m^2/g, pore volume of 0.49 cm^3/g and contains 50 ppm sulfur. The impregnated alumina was dried overnight at 353 K, then heated in air at 773 K for 3 h and finally reduced 2 h at 773 K in pure hydrogen.

Specific surface areas (S_g, m^2/g) were measured by N_2 physisorption at its boiling point using a Autosorb Quantochrome Instrument 1-C sorptometer and BET analysis methods. Prior to N_2 physisorption, the samples were outgassed for 1 h at 623 K. The Pt content of the samples were measured by inductively coupled plasma atomic emission spectroscopy (ICP-AES), using a Perkin–Elmer Optima 2100 unit. The Pt dispersion (D_{Pt}, surface Pt atoms/total Pt atoms) of the samples was determined by hydrogen chemisorption, using the double isotherm method as described in [22]. The volumetric adsorption experiments were performed in a conventional vacuum apparatus. Catalysts were reduced in H_2 at 673 K for 1 h and then outgassed 2 h at 673 K. After cooling to room temperature, a first isotherm was drawn for measuring the total H_2 uptake. Then, and after 1 h of evacuation at room temperature, a second isotherm was performed to determine the amount of weakly adsorbed hydrogen. The amount of irreversibly held hydrogen, $(HC)_i$, was calculated as the difference between total and weakly adsorbed hydrogen. The pressure range was 0–7 kPa and extrapolation to zero pressure was used as a measure of the H_2 uptake on the metal. A stoichiometric atomic ratio of H/Pt = 1 was used to determine the metal dispersion. Mean Pt crystallite sizes ($\overline{d}_{Pt}$, nm) were determined from H_2 chemisorption data by using site densities of 1.12×10^{15} sites per cm^2 of metal [23].

Catalysts III and IV were analyzed by transmission electron microscopy (TEM) using a JEOL 100 CX II microscope with an acceleration voltage of 100 KV and magnification of 450,000x. A significant number of Pt particles was observed to obtain reliable particle size distribution histograms. The average volume/area diameter of Pt crystallites (d_{VA}, nm) was calculated from $d_{VA} = \frac{\sum n_i d_i^3}{\sum n_i d_i^2}$, where n_i is the number of Pt particles of size d_i.

Powder X-ray diffraction patterns (XRD) were collected on a Shimadzu XD-D1 diffractometer using nickel filtered CuKα radiation. The acid properties of alumina support were determined by temperature-programmed desorption (TPD) of NH_3 preadsorbed at 373 K. Samples were pretreated in He at 773 K for 1.5 h and then exposed at 373 K to a flow of 1% NH_3/He for 40 min. Weakly adsorbed NH_3 was removed by flushing with He at 373 K for 0.5 h and then the temperature was increased at 10 K/min. The NH_3 concentration in the effluent was analyzed by mass spectrometry (MS) in a Baltzers Omnistar unit.

The nature of surface acid sites on alumina was determined by Fourier infrared transform spectroscopy (FTIR) of adsorbed pyridine using a Shimadzu FTIR–8101 M spectrophotometer. Samples were ground to a fine powder and pressed into wafers (20–40 mg). The discs were mounted in a quartz sample holder and transferred to an inverted T-shaped Pyrex cell equipped with CaF_2 windows. Samples were initially outgassed in vacuum at 723 K during 2 h and then a background spectrum was recorded after being cooled down to room temperature. Spectra were recorded at room temperature, after admission of pyridine, and degassing at 373 K.

The amounts of carbon formed on the catalysts during the catalytic tests were measured by temperature-programmed oxidation (TPO). Samples (50 mg) were heated in a 2% O_2/N_2 stream at 10 K/min from room temperature to 1073 K. The evolved CO_2 was converted to methane by means of a methanation catalyst (Ni/kieselghur) operating at 673 K and monitored using a flame ionization detector in an SRI 8610C gas chromatograph.

2.2. Catalytic tests

Catalytic tests for the APR of EG, Gly, Xyl and Sorb were carried out in a continuous packed-bed reactor at 498 K and 29.3 bar using aqueous solutions containing 1%wt polyol. Catalysts were sieved to retain particles with 0.35-0.42 mm diameter for catalytic measurements and reduced in hydrogen at 573 K for 1 h before reaction. The 1%wt polyol

solution was introduced to the reactor in a N_2 carrier flow (20 cm^3/min) using a HPLC-type pump (Alltech 310) and pressurized to setpoint. The reactor effluent was cooled down by passing through a condensation system and then conducted to a gas-liquid separator. A Shimadzu GC-2014 gas chromatograph equipped with a Hayesep D 100–120 column (5 m x 1/8 in x 2.1 mm), and thermal conductivity (TCD) and flame ionization (FID) detectors was used to analyze on line the gaseous products. Hydrogen was quantified using the TCD detector while CO, CO_2 and CH_4 were analyzed by FID after completely converting CO and CO_2 to methane by means of a methanation catalyst (Ni/Kieselghur) operating at 673 K. Condensable products were drained periodically and quantified by using high-performance liquid chromatography (HPLC) in a UFLC Shimadzu Prominence chromatograph equipped with a BioRad Aminex HPX-87C column (250 × 4.0 mm) and a refraction index detector (RID).

The total conversion of polyol P_n (X_{P_n}) to gaseous and liquid products was determined as:

$$X_{P_n} = \frac{F^0_{P_n} - F_{P_n}}{F^0_{P_n}} \tag{4}$$

where $F^0_{P_n}$ and F_{P_n} are the P_n molar flow at the inlet and the exit of the reactor, respectively. The carbon-based conversion of polyol P_n to gaseous products was calculated as:

$$X^G_{P_n} = \frac{\sum n_i F_i}{n_{P_n} F^0_{P_n}} \tag{5}$$

where n_i is the number of C atoms in the product i molecule, F_i the molar flow of gaseous product i formed from polyol P_n, and n_{Pn} the number of C atoms in the polyol P_n molecule.

The conversion of polyol P_n to liquid products, $X^L_{P_n}$, was calculated as the difference $X^G_{P_n}$ between X_{P_n} and

The yield to H_2 (Y_{H_2}, moles of H_2 produced/moles of polyol P_n fed) was calculated by considering the stoichiometric factors of reaction 3:

$$Y_{H_2} = \frac{F_{H_2}}{F^0_{P_n}} \cdot \frac{1}{2n+1} \tag{7}$$

The selectivity to H_2 in the gas phase is defined [3] as the number of moles of H_2 produced normalized by the number of moles of H_2 that would be present if each mole of carbon in the effluent gas had participated in the polyol reforming reaction to give (2n+1)/n mole of H_2. In our catalytic runs the amount of C_2–C_6 hydrocarbons in the gas phase was lower than 1% in all the cases, which is consistent with results reported in previous work on APR of polyols when no hydrogen is fed to the reactor [3,10], as is the case here. Then, the H_2 selectivity was determined as:

$$S_{H_2} = \frac{F_{H_2}}{F_{CO} + F_{CO_2} + F_{CH_4}} \cdot \frac{1}{RR} \tag{8}$$

where RR, the H_2/CO_2 reforming ratio, is (2n+1)/n and represents the maximum H_2/C molar ratio that can be obtained according to the stoichiometry of reaction 3. The H_2 productivity (Pr, mol H_2/h g_{cat}) was calculated as:

$$Pr = \frac{F_{H_2}}{W_{cat}} \tag{9}$$

The possibility of pore diffusion limitations was investigated by determining the value of Weisz-Prater parameter ϕ (eq. 10). According to the Weisz-Prater criterion [24], the internal diffusion limitations are negligible if $\phi < 1$ for a first order reaction or $\phi < 0.3$ for a second order reaction. Parameter ϕ is expressed by:

$$\phi = \frac{r_{obs} R_p^2}{C_{P_n} D_{eff}} \tag{10}$$

where r_{obs} (mol/cm^3 s) is the observed reaction rate, R_p (cm) the catalyst particle radius, C_{P_n}(mol/cm^3) the concentration of P_n, and D_{eff} (cm^2/s) the effective diffusivity of P_n in water. We determined the ϕ values corresponding to the maximum r_{obs} values obtained here at 498 K for the APR of our four polyols, using an average particle radium of R_p = 0.019 cm and the D_{eff} values calculated from the Wilke-Chang correlation [25]. The maximum value obtained for parameter ϕ was ϕ = 0.005, thereby indicating that the reaction rates reported here are not limited by internal mass transfer phenomena.

3. Results and discussions

3.1. Catalyst characterization

The alumina acid site density was obtained by TPD of NH_3. The NH_3 desorption rate curve (not shown here) presented a maximum at 500 K. The number of surface acid sites density determined from deconvolution and integration of the NH_3 TPD curve was 19 μmol NH_3/g, that is consistent with previous reports showing that commercial Al_2O_3 CK-300 is a medium-strength acid material [26,27].

The infrared spectrum of Al_2O_3 support obtained in the hydroxyl stretching region after evacuation at 723 K for 4 h showed that the hydroxyl group concentration was insignificant. Furthermore, the FTIR spectra of adsorbed pyridine confirmed that Al_2O_3 CK300 contains essentially Lewis acid sites [28].

The X-ray patterns (not shown) of our four Pt/A_2O_3 catalysts exhibited only the alumina crystalline structure which suggested that platinum was well dispersed on the support. The physicochemical properties of catalysts I, II, III and IV are presented in Table 1. The alumina impregnation with Pt nitrate solutions and the consecutive calcination and reduction steps involved in the catalyst preparation method did not change significantly the alumina surface area (220 m^2/g). The Pt dispersion as calculated by H_2 chemisorption diminished with the amount of metal from D_{Pt} = 67% on catalyst I to D_{Pt} = 54% on catalyst IV. Catalysts III and IV were also characterized by transmission electron microscopy; the corresponding TEM images and size distribution histograms were presented in a previous work [28]. The average volume/area diameter of Pt crystallites (d_{VA}) calculated by TEM were consistent with the mean crystallite sizes determined by H_2 chemisorption (Table 1).

3.2. Catalytic results

3.2.1. Effect of Pt loading on catalyst activity and selectivity

The catalytic properties of Pt/Al_2O_3 catalysts for APR of EG, Gly, Xyl and Sorb were evaluated at a space velocity of WHSV = 1.2 h^{-1}, 498 K and 29.3 bar. As an example, Fig. 2 shows the evolution of polyol conversion and H_2 yield and selectivity as a function of time on catalyst III for APR of EG and Gly. Stationary activity and selectivity values were obtained after about 2 h of time on stream; similar reaction start-up periods were observed on the other Pt/Al_2O_3 catalysts. The catalytic results reported here were all obtained from the stationary region of catalytic runs, typically illustrated in Fig. 2.

Table 1
Characteristics of Pt/Al_2O_3 catalysts used in this work.

Catalyst	Pt loading (wt%)	S_g (m^2/g)	$(HC)_i$ [a](μmol/g_{cat})	D_{Pt} [b](%)	Pt_s [c](μmol Pt/g_{cat})	$\bar{d}_{Pt}$ [b](nm)	d_{VA} [d](nm)
I	0.30	217	5.15	67	10.3	1.3	–
II	0.57	223	9.20	63	18.4	1.4	–
III	1.50	206	21.51	56	43.1	1.5	1.9
IV	2.77	209	38.00	54	76.7	1.6	2.0

[a] Irreversible H_2 uptake.
[b] Determined from $(HC)_i$ values.
[c] Surface Pt concentration.
[d] Determined by TEM.

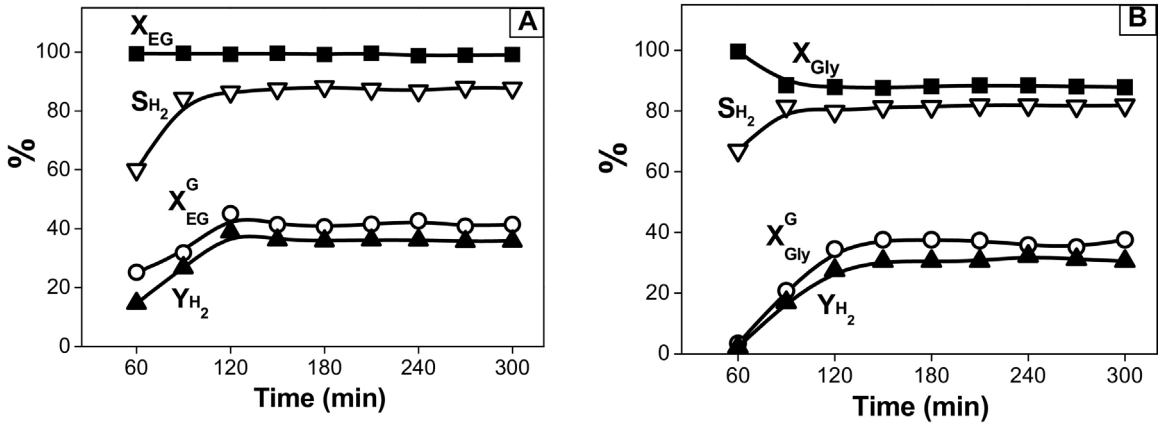

Fig. 2. Evolution of H_2 yield (Y_{H_2}), H_2 selectivity (S_{H_2}) and polyol conversions (X_{Pn}, X^G_{Pn}) as a function of time on stream for EG (A) and Gly (B).[Catalyst III, T = 498 K, P = 29.3 bar; WHSV = 1.2 h^{-1}, Feed: Polyol(1.0%)/water].

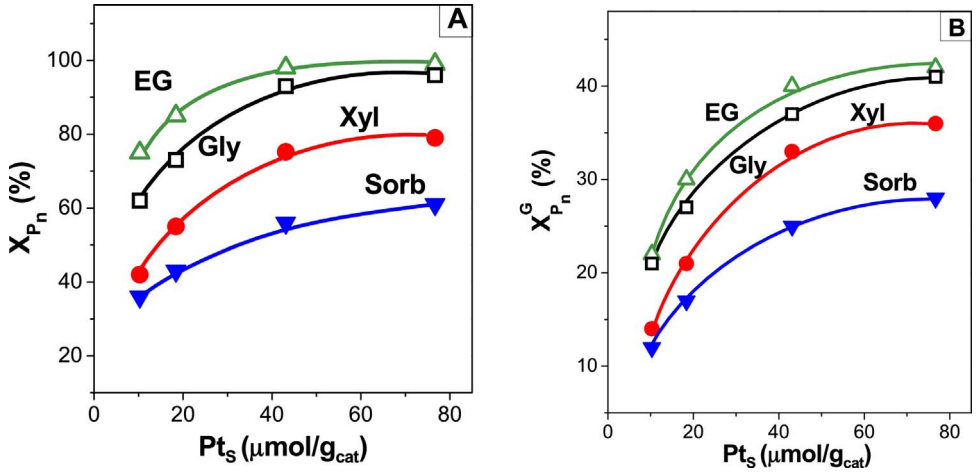

Fig. 3. Evolution of total conversion of polyol P_n (A) and conversion of P_n to gaseous products (B) as a function of surface Pt concentration.[T = 498 K, P = 29.3 bar; WHSV = 1.2 h^{-1}, Feed: Polyol(1.0%)/water].

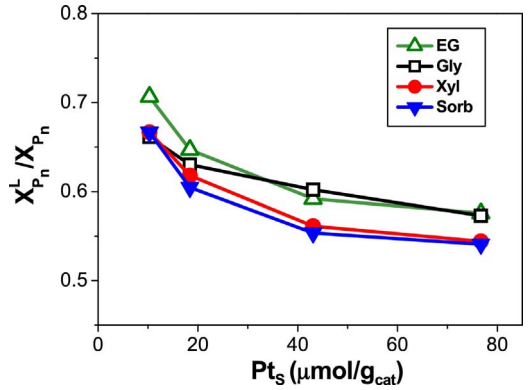

Fig. 4. Evolution of X^L_{Pn}/X_{Pn} ratio as a function of surface Pt concentration. Reaction conditions as in Fig. 3.

The effect of Pt loading on catalyst activity is shown in Fig. 3A and B, where we represented the evolution of total conversion of polyol P_n and P_n conversion to gaseous products, respectively, as a function of surface Pt concentration (Pt_s, Table 1). As shown in Fig. 3A, X_{P_n} increased continuously with Pt_s, which probably reflects the concomitant generation of surface metallic active sites; a similar activity increase was observed for $X^G_{P_n}$ vs Pt_s curves in Fig. 3B. At a given Pt_s value, X_{P_n} and $X^G_{P_n}$ decreased with the polyol chain length. Regarding the polyol conversion to liquid products, in Fig. 4 we plotted the $X^L_{P_n}/X_{P_n}$ ratio as a function of Pt_s; in all the cases, $X^L_{P_n}/X_{P_n}$ decreased when the amount of accessible Pt atoms was increased. From the results in Figs. 3 and 4, it is inferred then that the Pt loading increase on Pt/Al_2O_3 catalysts not only increases the polyol conversion rate but also the proportion of polyol converted to gaseous products. This later result is particularly important taking into account that the predominant polyol conversion to gaseous products is a requisite for improving the production of hydrogen.

The H_2 selectivity and the product composition in the gas phase obtained for the APR of EG, Gly, Xyl and Sorb on catalysts I (0.30% Pt) and IV (2.77% Pt) are presented in Table 2. The S_{H_2} values diminished with the polyol chain length, from 95% (EG) to 72% (Sorb) on catalyst I, and from 89% (EG) to 75% (Sorb) on catalyst IV; the H_2 concentration in the gas phase followed a similar trend. This relationship between S_{H_2} and the polyol size agrees with results reported in previous work showing that the H_2 selectivity decreases for the APR of polyols with larger carbon chains [3,10,29]. Regarding the effect of %Pt on H_2 selectivity, two phenomena must be considered to interpret the results reported in Table 2. First, the H_2 selectivity decreases when the polyol conversion increases because larger amounts of H_2 are consumed in hydrogenolysis and hydrogenation side-reactions at higher reactant conversion levels [30,31]. Second, at polyol isoconversion, the H_2 selectivity increases with surface Pt concentration on Pt/Al_2O_3 catalysts [28]. Results in Table 2 show that X_{P_n} is higher on catalyst IV which would result in a lower H_2 selectivity as compared to catalyst I; nevertheless, this expected drop in S_{H_2}may be partially compensated for the higher Pt content on catalyst IV that promotes better the H_2 production. Consistently, results in Table 2 shows that the H_2 selectiv-

Table 2
APR of polyols: Product distribution in the gas phase.

Polyol	Catalyst I						Catalyst IV					
	X_{P_n}	S_{H_2}	Gas composition (%, molar)				X_{P_n}	S_{H_2}	Gas composition (%, molar)			
			H_2	CO	CH_4	CO_2			H_2	CO	CH_4	CO_2
EG	75	95	70.5	0.1	0.4	29.0	97	89	69.1	0.1	0.4	30.4
Gly	62	90	67.9	0.3	5.9	25.9	96	86	66.7	0.5	4.4	28.4
Xyl	42	83	64.8	0.1	3.6	31.5	79	81	64.1	0.1	3.0	32.8
Sorb	36	72	60.9	0.6	4.0	34.5	61	75	61.8	0.2	3.2	34.8

[T = 498 K; P = 29.3 bar; WHSV = 1.2 h^{-1}; Feed: polyol(1.0%)/water].

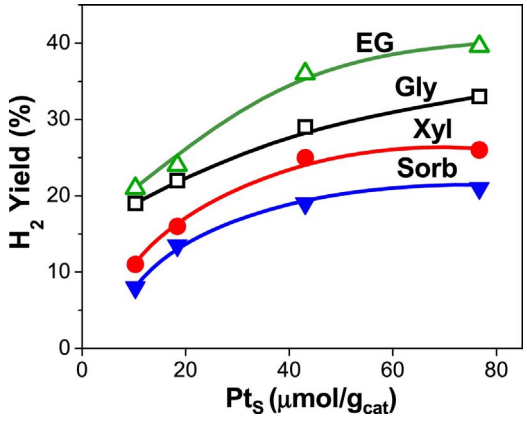

Fig. 5. H_2 yield vs Pt_s curves obtained for APR of EG, Gly, Xyl and Sorb. Reaction conditions as in Fig. 3.

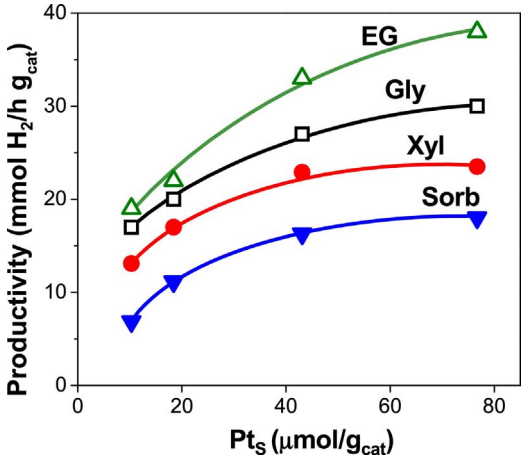

Fig. 6. H_2 productivity vs Pt_s curves obtained for APR of EG, Gly, Xyl and Sorb. Reaction conditions as in Fig. 3.

ities for each individual polyol are similar on catalyst I and IV.

Fig. 5 shows the evolution of the H_2 yield as a function of the Pt surface concentration for the APR of EG, Gly, Xyl and Sorb. In all the cases, Y_{H_2} increased continuously with Pt_s which essentially reflects the increase of X_{P_n} and $X_{P_n}^G$ with Pt_s observed in Fig. 3. At a given Pt_s value, Y_{H_2} decreased with the polyol size as it was expected tacking into account that X_{P_n} and $X_{P_n}^G$ (Fig. 3) and S_{H_2} (Table 2) decreased with the polyol chain length. Similar relationship between Y_{H_2} and the polyol size was reported by other authors [3,16].

From a commercial point of view, the most important parameter to evaluate the economy of the polyol APR process for producing hydrogen is the H_2 productivity, Pr (mol H_2/g_{cat} h), i.e. the average rate of H_2 production, that is expressed as:

$$Pr = \frac{F_{H_2}}{W_{cat}} = Y_{H_2} WHSV \frac{2n+1}{M_{P_n}} \quad (10)$$

where M_{P_n} is the molecular weight of polyol P_n. The *Pr* vs Pt_s plots obtained at WHSV = 1.2 h^{-1} for the APR of EG, Gly, Xyl and Sorb are presented in Fig. 6 and show that in all the cases the H_2 productivity increased with the surface Pt concentration. The highest H_2 productivities were then obtained here on catalyst IV (2.77% Pt). Actually, Eq. (10) predicts that *Pr* is proportional to Y_{H_2} at a constant WHSV value, so that the shape of *Pr* plots in Fig. 6 are similar to the shape of Y_{H_2} plots in Fig. 5. Also, the H_2 productivity follows the same trend than Y_{H_2} with respect to the polyol chain length, i.e. EG > Gly > Xyl > Sorb. It is significant noting in Fig. 6 that the *Pr* plots for polyols of 5 (Xyl) and 6 (Sorb) carbon atoms reached a plateau at $Pt_s \cong 45$ μmol/g_{cat} (catalyst III, containing 1.5% Pt) and no significant gain in H_2 productivity should be expected, then, when using Pt/Al_2O_3 catalysts containing higher Pt_s values. In contrast, the *Pr* plots corresponding to shorter polyols (Gly and EG) did not reach any plateau in Fig. 6 and higher H_2 productivities than those obtained here on catalyst IV (2.77% Pt, Pt_s = 76.7 μmol/g_{cat}) may be achieved by using Pt/Al_2O_3 catalysts containing surface Pt concentrations higher than 76.7 μmol/g_{cat}, in particular for EG.

3.2.2. Pt loading and coke formation

We also investigated the effect of surface Pt concentration on coke formation by determining by TPO technique the amount of carbon formed on Pt/Al_2O_3 catalysts recovered from the polyol APR catalytic runs performed at WHSV = 1.2 h^{-1} for 300 min. Before the TPO characterization, samples were treated at 523 K in N_2 during 60 min. Fig. 7 shows the TPO profiles obtained for samples recovered from the APR of EG, Gly, Xyl and Sorb. In general, the coke burnt gave rise to a broad asymmetric band between 500 and 850 K with a maximum at about 640–670 K for EG, Gly and Xyl that appeared shifted to lower temperatures (560–600 K) for Sorb. The shapes of TPO curves for each individual polyol did not change significantly with the Pt% on the catalyst. The amounts of carbon were calculated from the areas under the TPO curves of Fig. 7 and are presented in Table 3 as %C. A clear relationship between Pt_s and %C is observed in Table 3 for each individual polyol: the higher Pt_s, the higher the amount of carbon formed on the catalyst. This result may be explained by taking into account the plots in Fig. 3 showing that the polyol conversion increases with Pt_s; i.e. the higher X_{P_n} the higher the coke formation. Moreover, data in Table 3 also shows a clear trend between the polyol size and %C on a given Pt catalyst: the shorter the polyol chain length, the higher the amount of coke. Again, it must be noted here that the plots in Fig. 3 show that at a given Pt_s value, the polyol conversion increases for shorter substrates. In order to get more insight on the effect of Pt_s on coke formation, we calculated the number of carbon atoms formed per accessible Pt atom; results are presented in Fig. 8 as C/Pt_s vs Pt_s plots. Irrespective of the reactant size, the number of C atoms formed per accessible Pt atom decreased with Pt_s; in other words, one surface Pt atom forms lesser amounts of carbon when the Pt content on the catalyst is increased.

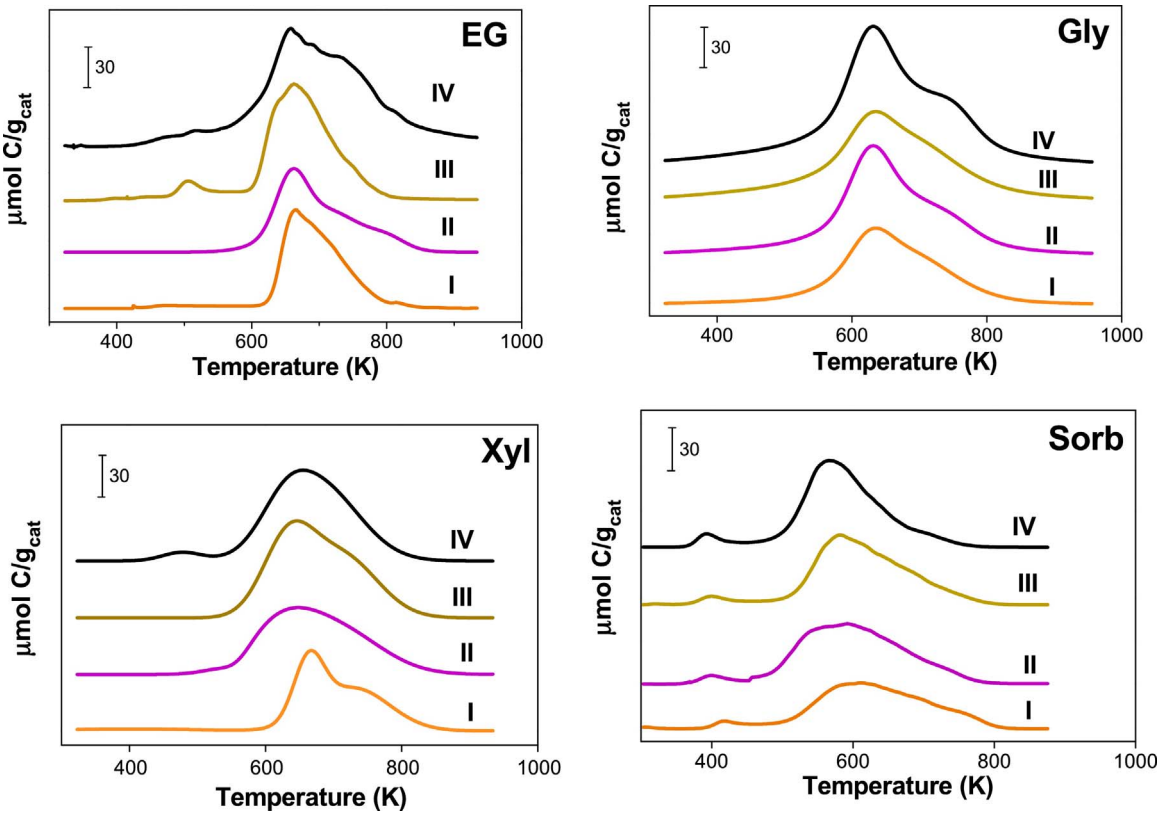

Fig. 7. TPO curves of catalysts I, II, III and IV recovered from APR of EG, Gly, Xyl and Sorb (reaction conditions as in Fig. 3).

Table 3
Amounts of coke formed on polyol APR runs.

Catalyst	Pt$_s$ (µmol Pt/g$_{cat}$)	%C			
		EG	Gly	Xyl	Sorb
I	10.3	1.03	0.97	0.94	0.67
II	18.4	1.29	1.27	1.16	0.82
III	43.1	1.49	1.41	1.36	0.89
IV	76.7	1.78	1.49	1.44	0.96

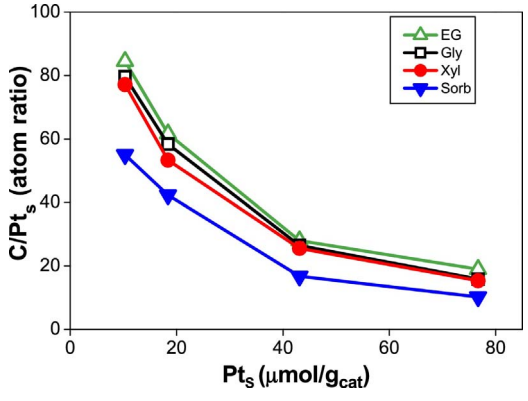

Fig. 8. Amounts of coke formed on polyol APR runs as a function of surface Pt concentration.

3.2.3. *Metal sintering of Pt/Al$_2$O$_3$ catalysts*

Finally, we investigated the sintering of Pt in Pt/Al$_2$O$_3$ catalysts during the polyol APR runs by determining the metallic dispersion of catalysts II, III and IV after reaction. At the end of catalytic tests for EG, Gly, Xyl and Sorb performed at WHSV = 1.2 h^{-1} for 300 min, we purged the reactor with nitrogen and then the catalysts were contacted

Table 4
Pt dispersion of Pt/Al$_2$O$_3$ catalysts before and after reaction.

Catalyst	Metal dispersión (D$_{Pt}$, %)					$D_{Pt}^{used}/D_{Pt}^{fresh}$			
	Fresh	Used							
		EG	Gly	Xyl	Sorb	EG	Gly	Xyl	Sorb
II	63	36	37	35	34	0.57	0.59	0.56	0.54
III	56	34	33	27	29	0.61	0.59	0.48	0.52
IV	54	28	31	26	26	0.52	0.57	0.48	0.48

[T = 498 K; P = 29.3 bar; WHSV = 1.2 h^{-1}, Feed: polyol(1.0%)/water, run length: 5 h].

with flowing air at 673 K for 3 h for eliminating adsorbed products and coke precursors. Then, we determined the platinum dispersion of the samples by H_2 chemisorption. In Table 4, we compare the D_{Pt} values obtained on fresh and used catalysts. Clearly, a significant Pt sintering was observed for all the catalysts, irrespective of the reactant size. Results in Table 4 are consistent with previous work reporting that the Pt particles of Pt/Al$_2$O$_3$ catalysts are severely sintered under APR reaction conditions [19,28]. A closer inspection of results in Table 4 reveals that the Pt sintering was not related to the size of the polyol molecule. For example, the $D_{Pt}^{used}/D_{Pt}^{fresh}$ ratio values on catalyst II for EG, Gly, Xyl and Sorb were 0.57, 0.59, 0.56 and 0.54, respectively. On the other hand, the magnitude of the D_{Pt} drop on stream seems not to be dependent either on the amount of platinum on Pt/Al$_2$O$_3$ catalysts. For example, results in Table 4 show that the $D_{Pt}^{used}/D_{Pt}^{fresh}$ ratio values on catalysts II, III and IV for the APR of glycerol were 0.59, 0.59 and 0.57, respectively. In spite of the loss of Pt surface area on stream, we did not detect any significant activity decay once the stationary operating conditions were reached in the standard catalytic runs of 5 h length, as illustrated in Fig. 2. Additional catalytic tests of 36 h performed for APR of xylitol and sorbitol on catalyst III confirmed that the catalyst activity remained constant during the APR reaction. These results suggest that

the Pt sintering probably takes place mainly during the catalyst work-up, i.e. at the start of the APR reaction (Fig. 2). In order to check this assumption, we carried out three catalytic runs of 1 h, 2 h and 3 h length for APR of EG on catalyst IV (D_{Pt} = 54%) and then we measured the Pt dispersion after reaction. The obtained D_{Pt} values were 27%, 31% and 29% for the APR reactions of 1, 2, and 3 h, respectively, which confirmed that the Pt sintering occurs mostly in the start-up of the APR reaction, when the Pt/Al_2O_3 catalysts are initially contacted at 498 K with the polyol(1%)/water feed stream.

4. Conclusions

The production of hydrogen by aqueous-phase reforming of C_2−C_6 polyols on Pt/Al_2O_3 catalysts containing 0.30–2.77 Pt% depends on the surface Pt concentration (Pt_s) and the polyol size. The conversion of C_2−C_6 polyols to gaseous products, and the H_2 yield and productivity (*Pr*) increase with Pt_s and using shorter substrates. The H_2 productivity increases continuously with Pt_s but reached a plateau for xylitol and sorbitol at about 45 μmol Pt/g_{cat}; in contrast, no saturation of *Pr* vs Pt_s plots was observed here for glycerol and ethylene glycol when using Pt/Al_2O_3 catalysts containing up to 76.7 μmol Pt/g_{cat}. Similarly, the amount of coke formed on the catalysts increases with Pt_s and for smaller polyols, probably reflecting the parallel increase of the polyol conversion with both parameters.

A severe Pt sintering takes place during the APR of polyols, irrespective of the polyol chain length. The magnitude of the Pt area drop on stream seems not to be dependent on the amount of platinum on Pt/Al_2O_3 catalysts. Short-terms catalytic runs performed for APR of ethylene glycol, suggest that the Pt sintering occurs essentially during the start-up of the APR reaction, when Pt/Al_2O_3 catalysts are initially contacted at 498 K with the polyol(1%)/water feed stream.

Acknowledgements

Authors thank the Universidad Nacional del Litoral (UNL), Consejo Nacional de Investigaciones Científicas y Técnicas (CONICET), and Agencia Nacional de Promoción Científica y Tecnológica (ANPCyT), Argentina, for the financial support of this work

References

[1] H. Balat, E. Kirtay, Int. J. Hydrogen Energy 35 (2010) 7416.
[2] I. Coronado, M. Stekrova, M. Reinikainen, P. Simell, L. Lefferts, J. Lehtonen, Int. J. Hydrogen Energy 41 (2016) 11003.
[3] R.D. Cortright, R.R. Davda, J.A. Dumesic, Nature 418 (2002) 964.
[4] J.W. Shabaker, R.R. Davda, G.W. Huber, R.D. Cortright, J.A. Dumesic, J. Catal. 215 (2003) 344.
[5] R.R. Davda, J.W. Shabaker, G.W. Huber, R.D. Cortright, J.A. Dumesic, Appl. Catal. B: Environ. 56 (2005) 171.
[6] J.W. Shabaker, G.W. Huber, R.R. Davda, R.D. Cortright, J.A. Dumesic, Catal. Lett. 88 (2003) 1.
[7] G.W. Huber, J.W. Shabaker, S.T. Evans, J.A. Dumesic, Appl. Catal. B: Environ. 62 (2006) 226.
[8] K. Lehnert, P. Claus, Catal. Commun. 9 (2008) 2543.
[9] A. Wawrzetz, B. Peng, A. Hrabar, A. Jentys, A.A. Lemonidou, J.A. Lercher, J. Catal. 269 (2010) 411.
[10] A.V. Kirilin, A.V. Tokarev, L.M. Kustov, T. Salmi, J.P. Mikkola, D.Yu. Murzin, Appl. Catal. A: Gen. 435–436 (2012) 172.
[11] A.V. Kirilin, A.V. Tokarev, H. Manyar, C. Hardacre, T. Salmi, J.P. Mikkola, D.Yu. Murzin, Catal. Today 223 (2014) 97.
[12] A.V. Kirilin, J. Wärna, A.V. Tokarev, D.Yu. Murzin, Ind. Eng. Chem. Res. 53 (2014) 4580.
[13] A.V. Kirilin, A.V. Tokarev, E.V. Murzina, L.M. Kustov, J.P. Mikkola, D.Yu. Murzin, ChemSusChem 3 (2010) 708.
[14] A. Tanksale, Y. Wong, J.N. Beltramini, G.Q. Lu, Int. J. Hydrogen Energy 32 (2007) 717.
[15] G.W. Huber, J.A. Dumesic, Catal. Today 111 (2006) 119.
[16] T.W. Kim, M.C. Kim, Y.C. Yang, Y.R. Kim, S.Y. Jeong, C.U. Kim, Int. J. Hydrogen Energy 40 (2015) 15236.
[17] R.R. Davda, J.W. Shabaker, G.W. Huber, R.D. Cortright, J.A. Dumesic, Appl. Catal. B: Environ. 43 (2003) 13.
[18] G.W. Huber, R.D. Cortright, J.A. Dumesic, Angew. Chem. Int. Ed. 43 (2004) 1549.
[19] T.W. Kim, H.D. Kim, K.E. Jeong, H.J. Chae, S.Y. Jeong, C.H. Lee, C.U. Kim, Green Chem. 13 (2011) 1718.
[20] W. Yamaguchi, Y. Tai, Chem. Lett. 43 (2014) 313.
[21] H.A. Duarte, M.E. Sad, C.R. Apesteguia, Int. J. Hydrogen Energy 41 (2016) 17290.
[22] A. Borgna, T.F. Garetto, C.R. Apesteguia, F. Le Normand, B. Moraweck, J. Catal. 86 (1999) 433.
[23] T.F. Garetto, C.R. Apesteguía, Catal. Today 62 (2000) 189.
[24] P.B. Weisz, C.D. Prater, Adv. Catal. 6 (1954) 143.
[25] C.R. Wilke, P. Chang, AIChE J. 1 (1955) 264.
[26] T.F. Garetto, E. Rincón, C.R. Apesteguía, Appl. Catal. B: Environ. 73 (2007) 65.
[27] N.M. Bertero, A.F. Trasarti, C.R. Apesteguía, A.J. Marchi, Appl. Catal. A: Gen. 458 (2013) 28.
[28] H.A. Duarte, M.E. Sad, C.R. Apesteguia, Int. J. Hydrogen Energy 42 (2017) 4051.
[29] H.D. Kim, H.J. Park, T.W. Kim, K.E. Jeong, H.J. Chae, S.Y. Jeong, C.H. Lee, C.U. Kim, Catal. Today 185 (2012) 73.
[30] M.F. Neira D'Angelo, J.C. Schouten, J. van der Schaaf, T.A. Nijhuis, Catal. Sci. Technol. 3 (2013) 2834.
[31] N. Li, G.W. Huber, J. Catal. 270 (2010) 48.